

# Conformation Governed Reactivity of Fused Thia-Sapphyrin Dimers Bearing Multiply Fused Heteroaromatic Rings

Qizhao Li<sup>1\*</sup>, Masatoshi Ishida<sup>2</sup>, Chengjie Li<sup>1</sup>, Glib Baryshnikov<sup>3</sup>, Feng Sha<sup>1</sup>, Bin Zhu<sup>1</sup>, Xinyan Wu<sup>1</sup>, Hans Ågren<sup>4</sup>, Hiroyuki Furuta<sup>5,6\*</sup> & Yongshu Xie<sup>1</sup>

<sup>1</sup>Key Laboratory for Advanced Materials and Joint International Research Laboratory of Precision Chemistry and Molecular Engineering, Feringa Nobel Prize Scientist Joint Research Center, Frontiers Science Center for Materiobiology and Dynamic Chemistry, Institute of Fine Chemicals, School of Chemistry and Molecular Engineering, East China University of Science and Technology, Shanghai 200237, <sup>2</sup>Department of Chemistry, Graduate School of Science, Tokyo Metropolitan University, Tokyo 192-0397, <sup>3</sup>Department of Science and Technology, Laboratory of Organic Electronics, Linköping University, Norrköping SE-60174, <sup>4</sup>Department of Physics and Astronomy, Uppsala University, Uppsala SE-751 20, <sup>5</sup>Department of Applied Chemistry, Graduate School of Engineering, Kyushu University, Fukuoka 819-0395, <sup>6</sup>Research Organization of Science and Technology, Ritsumeikan University, Kusatsu 525-8577

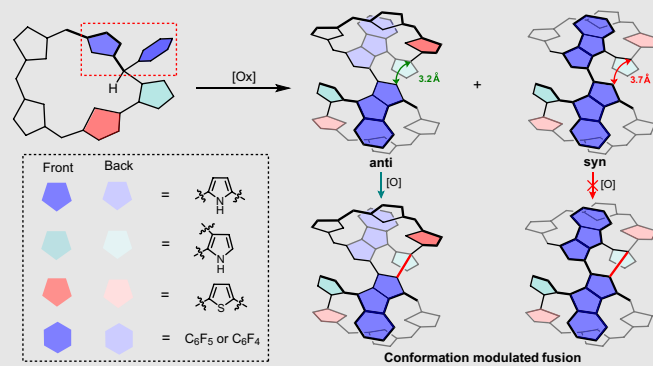
\*Corresponding authors: [zhaolq@ecust.edu.cn](mailto:zhaolq@ecust.edu.cn); [furuta.hiroyuki.165@m.kyushu-u.ac.jp](mailto:furuta.hiroyuki.165@m.kyushu-u.ac.jp)

Cite this: CCS Chem. 2023, 5, 1332-1342

DOI: 10.31635/ccschem.023.202202690

Suitable conformations and proper alignment of complex natural macrocycles are essential for achieving their unique properties. However, such artificial macrocycle prototypes are still limited due to synthetic difficulties. In this respect, directly linked porphyrin analog dimers display tunable conformations and intriguing properties, and thus, they may be employed as a class of promising platforms. Herein, we report that one-pot oxidative dimerization of thia-hydrosapphyrin 1 yields dimers,  $2_{\text{anti}}$  and  $2_{\text{syn}}$ , comprising a *transoid*-oriented plate-like bipyrrolo[1,2-a]indolylidene. The thiophene-containing tetrapyrrole arching subunits in  $2$  lie at the opposite (*anti*) and same (*syn*) sides of the plate, respectively. Meanwhile, multiply fused *cisoid*-orientated dimer  $3$  was also obtained; a polycyclic pyrrolo-bridged bipyrroloindole derivative tethered with fully  $\pi$ -conjugated bridges was formed. Notably, the *anti*-dimer  $2_{\text{anti}}$  underwent subsequent oxidative fusion to furnish a further-fused [6.5.5.7.5.5.6]-octacyclic compound  $4_{\text{anti}}$ . In contrast, the *syn*-orientated  $2_{\text{syn}}$  could not be further fused due to the long distance between the

potential reaction sites. This study provides a unique approach to the fused dimeric porphyrin analogs for potential near-infrared optical materials by a simple oxidation reaction. It also reveals the importance of conformation-modulated reactivity for constructing complex porphyrin arrays.



**Keywords:** porphyrins, porphyrinoids, sapphyrins,  $\pi$ -conjugated systems, porphyrin oligomers, near-infrared dyes, macrocycles

## Introduction

Complex macrocycles and related supramolecular systems are ubiquitous structural motifs in natural systems. Multiple scientific communities are interested in mimicking and surpassing their distinctive properties.<sup>1–3</sup> For various natural systems, suitable conformations and proper alignment of the macrocycles often play key roles in their chemical reactivities and physicochemical properties.<sup>4–7</sup> However, because of synthetic difficulties, the structure–property correlation has not been fully revealed due to the lack of proper artificial macrocycle prototypes.<sup>6–9</sup>

As a representative class of  $\pi$ -conjugated compounds, the naturally occurring porphyrins and their analogs have attracted extensive interest because of their biological relevance and interesting photophysical and

electronic properties applicable in various research fields.<sup>10–13</sup> In particular, directly connected (and fused) porphyrin arrays are potential functional materials that show near-infrared (NIR) optical features, multiple redox responses, nonlinear optical properties, and so on.<sup>14–16</sup> To date, many directly coupled porphyrin dimers have been reported by oxidative reactions (Figure 1a).<sup>17–21</sup> However, the rigid and planar conformations of porphyrin macrocycles are difficult to modulate and thus limit the relevant research on the conformation-dependent properties. To address this problem, nonplanar porphyrin analogs, that is, porphyrinoids, may be employed to construct the corresponding dimers as promising artificial platforms.

The coupling reaction of aromatic compounds using an oxidant is one of the most straightforward synthetic strategies for achieving the desired-array structures from suitable monomeric precursors.<sup>22,23</sup> Such reactions usually

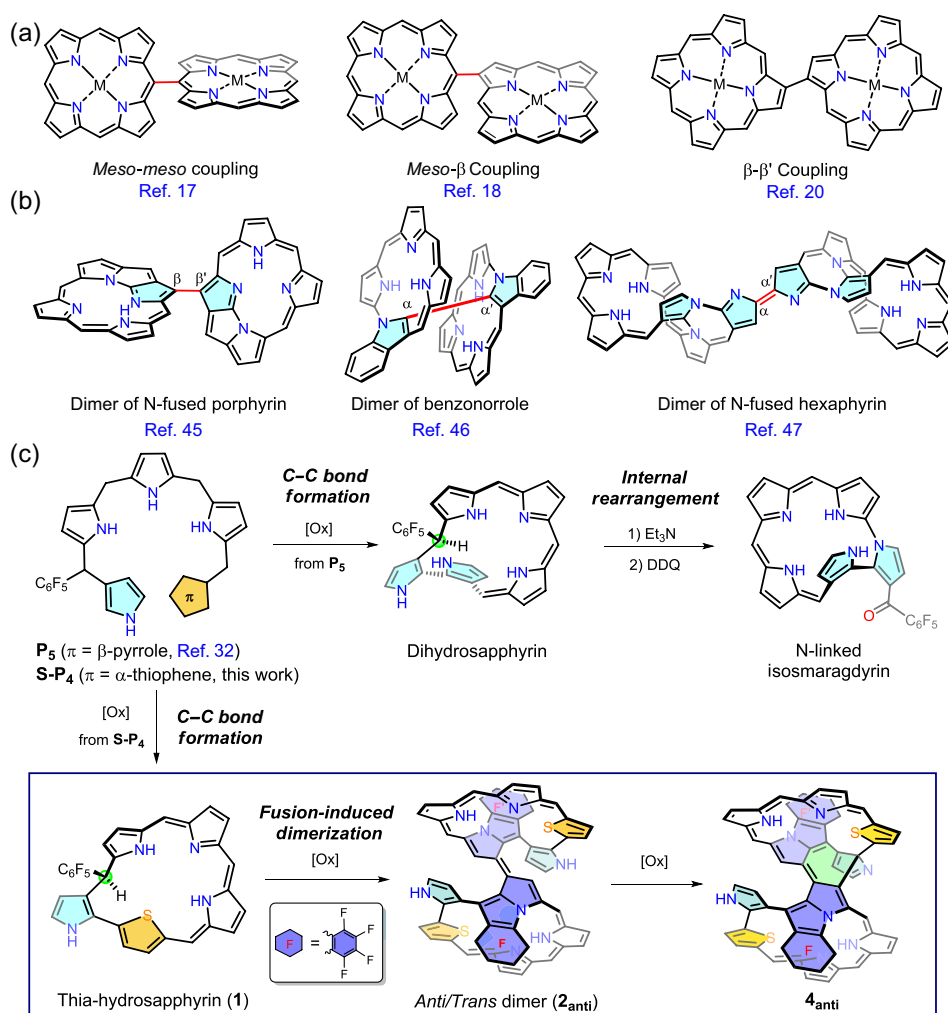


**Figure 1 |** (a) Representative oxidatively coupled porphyrin arrays. (b) Structures of pyrrole-pyrrole linked dimeric species based on mislinked porphyrinoids. (c) Overview of the oxidative cyclization and subsequent macrocyclic transformation of oligopyrroles with terminal  $\beta$ -pyrrolyl/thienyl units.

proceed through the radical mechanism if the substrate is reasonably electron rich. In this regard, porphyrins and their analogs are suitable platforms for stabilizing various electronic states, including open-shell radical species, which offer specific reactivity.<sup>24,25</sup> Because the regioselectivity of the oxidative coupling reactions strongly depends on the distinct electronic structure (i.e., electron density) and steric factors, the elaborately designed porphyrin analogs with mislinked pyrrole units (e.g.,  $\alpha$ - $\beta$ ,  $\alpha$ - $\beta'$ , or N- $\beta$  modes) in the corresponding scaffolds show selective reactivity.<sup>26-32</sup> Thus, chemical oxidation of N-confused porphyrin,<sup>33,34</sup> N-fused porphyrin,<sup>35-38</sup> neo-confused corrole (norrole),<sup>39-42</sup> and neo-confused hexaphyrin,<sup>43,44</sup> afforded the three-dimensional dimeric structures<sup>45-50</sup> with high regioselectivity via dehydrogenative C-C bond formation (Figure 1b).

In this regard, we have previously demonstrated that the cyclization of a pentapyrrane with two terminal  $\beta$ -pyrrolyl units (**P<sub>5</sub>**) afforded a highly twisted dihydrosapphyrin possessing a *meso*-sp<sup>3</sup>-carbon atom, which exhibited an unusual skeletal transformation reaction (Figure 1c).<sup>32</sup> To extend a divergent N-confusion strategy, we herein report the cyclization and subsequent dimerization of a hetero-pentapyrrane (**S-P<sub>4</sub>**) containing terminal  $\alpha$ -thienyl and  $\beta$ -pyrrolyl units to afford sets of fused dimers bearing a bipyrroloindolyl moiety with double  $\pi$ -conjugated straps. Therefore, upon cyclization, the incorporated  $\alpha$ -linked thienyl unit makes a coplanar pyrrole-thiophene geometry, leading to spatial proximity between the pyrrole and the adjacent *meso*-pentafluorophenyl ring.<sup>51-53</sup> In addition, the thiophene ring has a higher extent of 6 $\pi$  aromaticity than the pyrrole unit, leading to chemical stabilization. Thus, the local N-fusion forms the tricyclic aza-benzopentalenyl moiety protruding from the macrocycle, affording unusual dimers (i.e., **2**) by radical-mediated oxidative reactions (Figure 1c).<sup>54</sup> Notably, the stereoisomeric **2<sub>anti</sub>** and **2<sub>syn</sub>** exhibit distinct shape-pertinent reactivity; only **2<sub>anti</sub>** afforded a further-fused product (**4<sub>anti</sub>**), comprising a multiply fused [6.5.5.7.5.5.6]-octacyclic moiety surrounded by the  $\pi$ -conjugated arches. These heterocyclic aromatic hydrocarbons with arched  $\pi$ -conjugated bridges demonstrated unique NIR optical features upon protonation.

## Experimental Methods

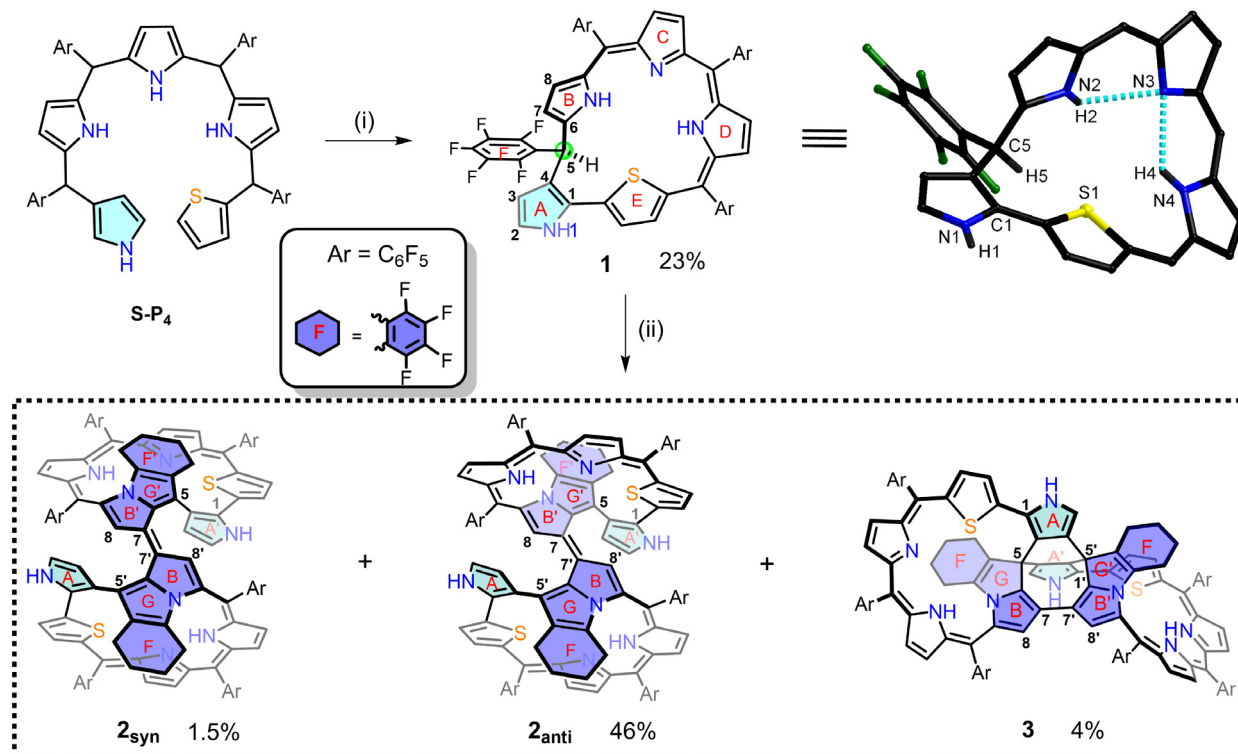
Commercially available solvents and reagents of analytical grade were used without further purification unless otherwise mentioned. The experimental details are provided in the Supporting Information, including the general experimental instruments, testing methods, theoretical calculation details, and the synthetic processes and structural characterization of the compounds.

## Results and Discussion

### Syntheses, characterization, crystal structures, and aromaticity

The synthetic details are outlined in Scheme 1. The key precursor thienyl-tetrapyrrole **S-P<sub>4</sub>** was prepared through a [2+3] condensation route (see Supporting Information Figures S1, S3, and S23). Direct oxidation of **S-P<sub>4</sub>** with various oxidants like 2,3-dichloro-5,6-dicyano-*p*-benzoquinone (DDQ) and *p*-chloranil afforded unidentified mixtures of highly polar compounds. Considering the possible template effect on the cyclization of oligopyrranes,<sup>55-58</sup> we tried various metal ions. We found that zinc acetate afforded the desired cyclization product **1** (Supporting Information Figure S24) in a reasonable yield (23%). Single-crystal X-ray diffraction analysis of **1** demonstrated a non-globally conjugated structure containing an sp<sup>3</sup>-hybridized carbon (C5) (Scheme 1) as similar to the corresponding dihydrosapphyrin (Supporting Information Figures S7, S8, and S29).<sup>32</sup> The confused pyrrole (ring A) is directly linked to the  $\alpha$ -position of thiophene (ring E). Consistent with the crystal structure, the 1D and 2D <sup>1</sup>H NMR spectra of **1** in acetone-*d*<sub>6</sub> indicated distinctive nonaromatic features. The peripheral CH signals are observed in the range of 5.79–6.94 ppm, and the characteristic singlet signal at 7.89 ppm can be assigned to be the *meso*-sp<sup>3</sup> CH (Supporting Information Figures S3–S6).

Considering the presence of a *meso*-sp<sup>3</sup> CH in **1**, it was treated with common oxidants to check whether it can be oxidized to fully conjugated molecules.<sup>28,32</sup> Interestingly, heating **1** in *N,N*-dimethylformamide (DMF) under aerobic conditions afforded three fused dimeric species, **2<sub>anti</sub>**, **2<sub>syn</sub>**, and **3**, in yields of 46%, 1.5%, and 4%, respectively. The high-resolution electrospray ionization mass spectrometry (HR-ESI-MS) analysis of **2<sub>anti</sub>** and **2<sub>syn</sub>** demonstrated almost identical molecular ion peaks at 2073.0876 and 2073.0874 ([M + H]<sup>+</sup>, calcd for C<sub>96</sub>H<sub>23</sub>F<sub>38</sub>N<sub>8</sub>S<sub>2</sub>: 2073.0880), respectively, indicating dimeric structures along with the elimination of two fluorine and eight hydrogen atoms (Supporting Information Figures S25 and S26). The HR-ESI-MS of **3** exhibited the molecule ion peak at 2071.0715 ([M + H]<sup>+</sup>, calcd for C<sub>96</sub>H<sub>21</sub>F<sub>38</sub>N<sub>8</sub>S<sub>2</sub>: 2071.0724) (Supporting Information Figure S27), indicative of a further-fused dimeric structure (Supporting Information Figure S17). To probe the effect of dimerization conditions on the yields of the dimers, the DMF solution of **1** was purged of air and heated under N<sub>2</sub> atmosphere, which resulted in negligible dimers, suggesting that air is essential for generating the dimers. To further check the effect of the oxidant, **1** was heated in DMF with *p*-chloranil under N<sub>2</sub> atmosphere. Dimers **2<sub>anti</sub>** and **4<sub>anti</sub>** (vide infra) were generated, whereas no **2<sub>syn</sub>** or **3** could be detected. When stronger oxidants like DDQ or Ag(I) salts were added slowly into the solutions of **1**, only



complicated mixtures of highly polar compounds could be obtained, and no stable products could be isolated. However, formation of the dimers is accompanied by simultaneous removal of hydrogen and fluorine atoms, which may involve the elimination of hydrogen fluoride (HF) molecules (vide infra, Supporting Information Figure S34), and thus it is anticipated that bases may be favorable for such dimerization reactions. Moreover, the addition of bases like  $Et_3N$  and  $NaOH$  indeed accelerated the reactions, whereas the yields of the dimers were noticeably lower due to more side products. Based on these results, the optimized condition for the dimerization reactions is to heat **1** in  $DMF$  under aerobic conditions without adding any base or other oxidants.

Dimer **2<sub>anti</sub>** contains an (*E*)-1,1'-bipyrrolo[1,2-*a*]indolylidene core with two  $\pi$ -conjugated thia-tetrapyrin arches directly linked at the C5/C5' and C9/C9' positions (Figure 2a,e,l and Supporting Information Table S1), which was constructed by the defluorinated N-fusion reaction between the *meso*-pentafluorophenyl group (ring F) and the neighboring pyrrole (ring B), followed by oxidative CH coupling at the outward C7 position. The macrocyclic arches lie in the *anti*-fashion to the mean plane of the bipyrrole-indolylidene core through the double-bond linkage at C7-C7' (1.385(3) Å) (Supporting Information Figure S30).

A similar reaction mode was observed in generating **2<sub>syn</sub>**. However, unlike **2<sub>anti</sub>**, two heteropyrrolic arching subunits lie at the same (*syn*) side of the central core. Due to the *syn* orientation, the fused FGB-B'G'F' core is bent with a torsion angle of 18.8° (Figure 2b,f,j).

Consistent with the non-interconvertible orientation of the arch moieties associated with the steric hindrance, the *syn/anti*-structural symmetry is reflected by the subtle difference between the  $^1H$  NMR spectra of **2<sub>anti</sub>** and **2<sub>syn</sub>** (Supporting Information Figures S9 and S14). Notably, the CH signals of C8(C8') in **2<sub>anti</sub>** and **2<sub>syn</sub>** appear at 5.75 and 5.33 ppm, respectively, and they are highly shielded due to the local ring current proximity of the confused pyrrole (rings A and A') (Supporting Information Figures S11 and S16). The nucleus-independent chemical shift (NICS) values<sup>59</sup> are consistent with the weakly aromatic quinoidal-like electronic structure of the aza-pentalenylidene core (rings B, G, B', and G') in the central scaffold (Figure 2i,j). The outer CH protons of **2<sub>anti</sub>** and **2<sub>syn</sub>** lie in the typical alkene regions of 5.75–7.18 and 5.33–6.96 ppm (Supporting Information Figures S9–S16), respectively, suggesting the nonaromatic character of **2<sub>anti</sub>** and **2<sub>syn</sub>**. To further elucidate the nonaromatic character, anisotropy of the induced current density (ACID)<sup>60</sup> plots of **2<sub>anti</sub>** and **2<sub>syn</sub>** were calculated, and no obvious clockwise or

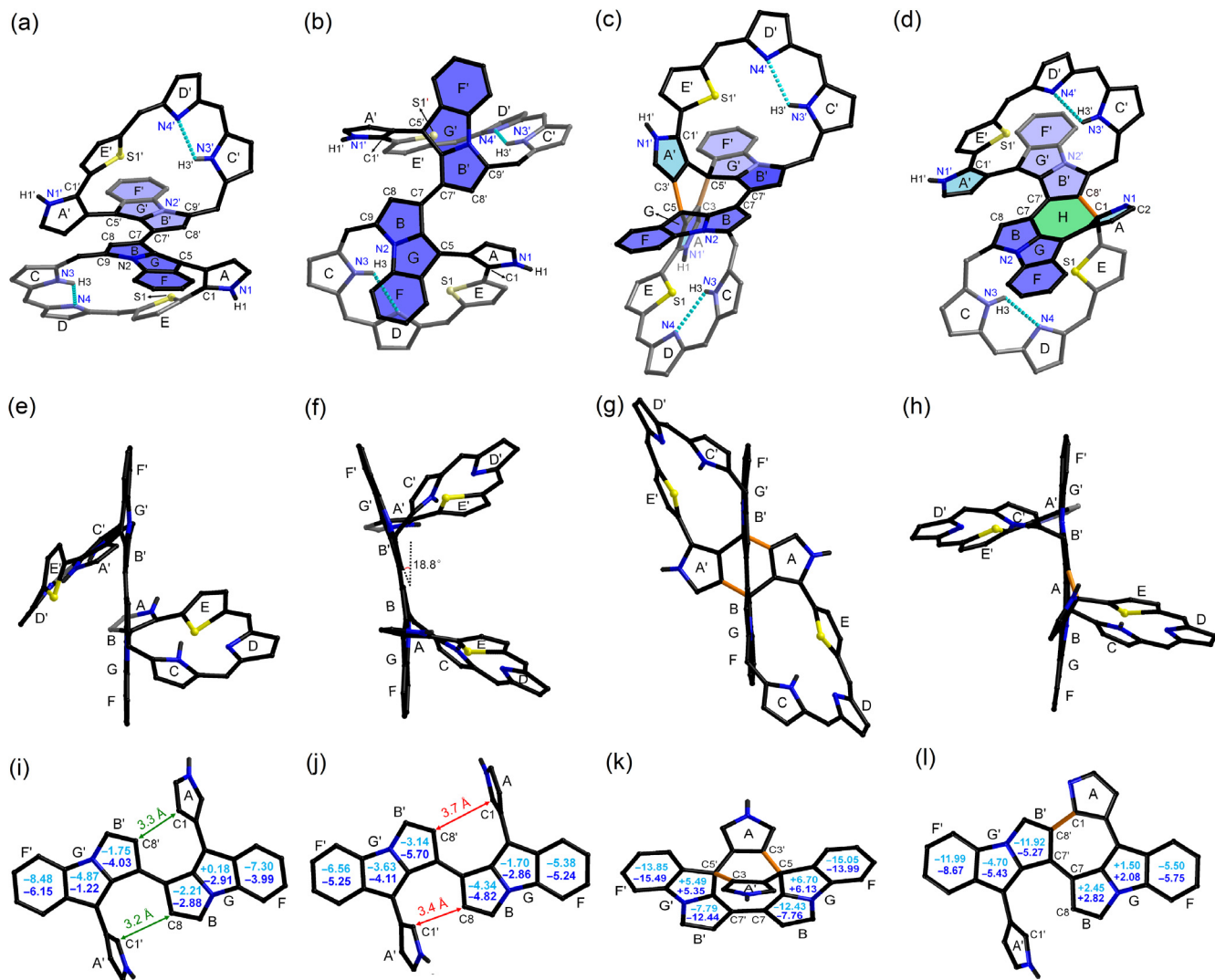


**Figure 2 |** Perspective molecular structures of **2<sub>anti</sub>** (a, e), **2<sub>syn</sub>** (b, f), **3** (c, g), and **4<sub>anti</sub>** (d, h).  $C_6F_5$  groups and hydrogen atoms attached to carbon atoms are omitted for clarity. The dotted lines represent hydrogen bonds. (i-l) The NICS(1)<sub>zz</sub> (cyan) and NICS(-1)<sub>zz</sub> (blue) values of the fused cores of **2<sub>anti</sub>**, **2<sub>syn</sub>**, **3**, and **4<sub>anti</sub>**, with the distances between the potential reaction sites indicated by the values above the arrows in panels (i) and (j).

counterclockwise current was observed from the ACID plots (Supporting Information Figure S38). In addition, the NICS(0) values around the cavity center were calculated to be  $-0.23$  and  $-0.61$ , respectively, in agreement with the nonaromatic character of **2<sub>anti</sub>** and **2<sub>syn</sub>**.

In contrast to the *transoid* isomers of **2<sub>anti</sub>** and **2<sub>syn</sub>**, aza-benzopentalenylidene moieties (BGF and B'G'F') within **3** are oriented in a *cisoid* configuration (Figure 2c,g), and the parts of the two conjugated arches lie at opposite sides of the core. The confused pyrrole rings participate in further fusion to generate a bicyclo[4.2.2]deca-2,4-diene structure by forming the bonds C3-C5' and C3'-C5. Moreover, the C7-C7' bond length of  $1.461(1)$  Å is longer than the corresponding values of  $1.385(3)$  and  $1.443(6)$  Å for the double bond linkage within dimers **2<sub>anti</sub>** and **2<sub>syn</sub>**, respectively.

(Supporting Information Figures S30-S32). The resulting structural change in the bipyrrole-indolylidene moieties is reflected in the distinct NICS(1/-1) values of the core moieties (B, G, and F) (Figure 2k).

### Plausible mechanism

For the conversion reactions from monomer **1** to dimers **2** and **3**, we speculated the involvement of radical intermediates (Figure 3 and Supporting Information Figure S34). As expected, the dimerization was disturbed by the radical scavenger 2,2,6,6-tetramethylpiperidine (TEMPO). Therefore, the N-C fusion reaction with the meso- $C_6F_5$  group may lead to the fused radical species **5** (Scheme 2). The possible radical species **5** could undergo further self-dimerization to afford the dimeric

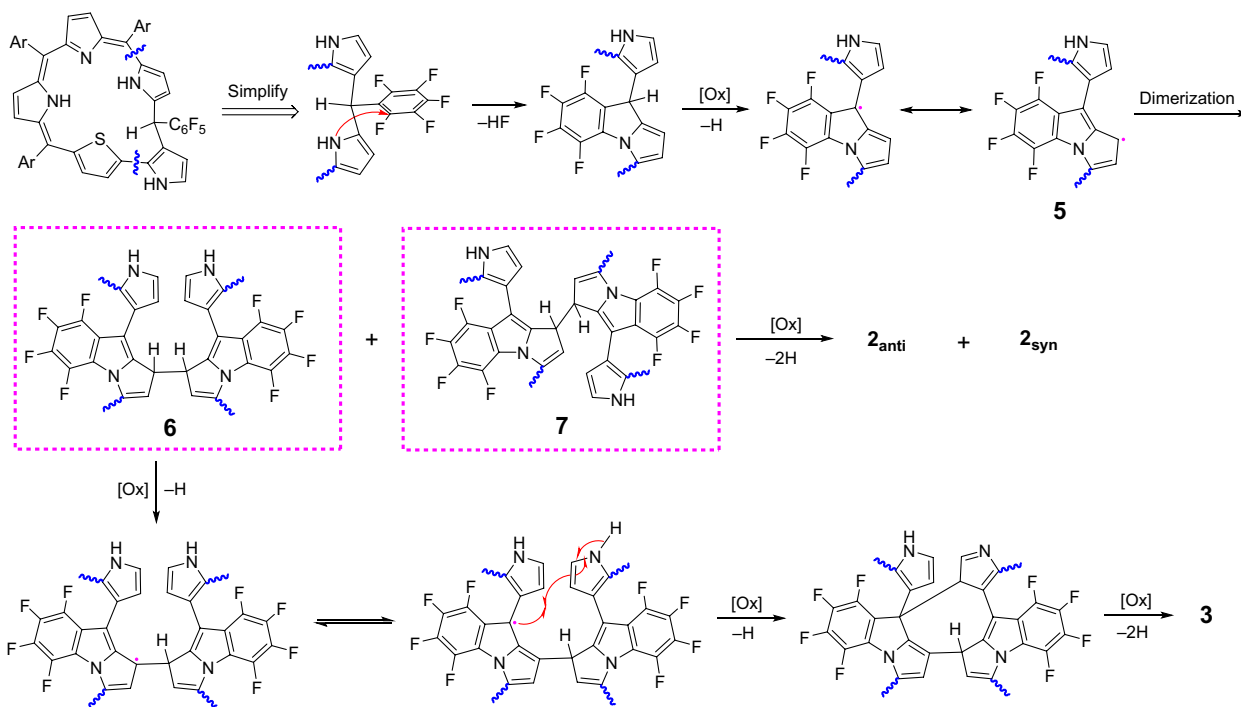
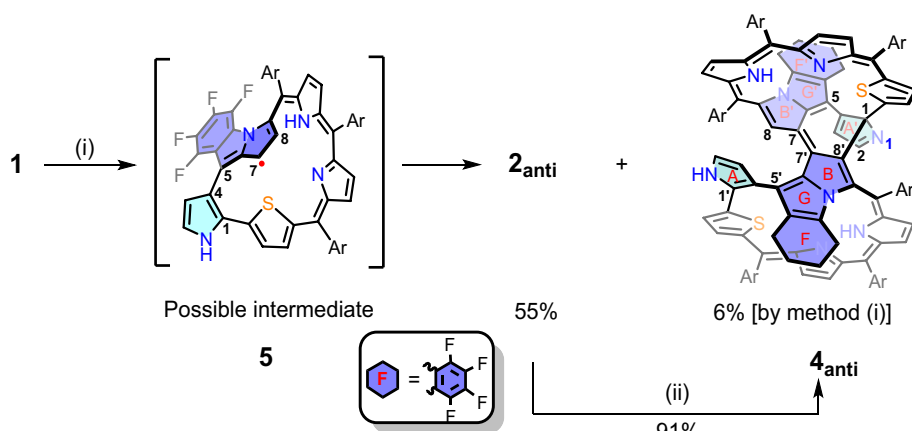


**Figure 3** | Plausible mechanisms proposed for generating **2** and **3** from **1** by oxidation.

intermediates **6** and **7**. The spin density map of **5**, which shows a higher coefficient at the less hindered C7 position of the aza-benzopentalenylidene moiety, indicated the regioselectivity of the self-dimerization (Supporting Information Figure S34). The *cis* conformation of **6** would be favorable for the radical oxidation to form **3** by removing four hydrogens. Meanwhile, the *trans* conformation of **7** would be favorable for the radical oxidation to form **2** by removing two hydrogens directly. In addition, compared to **2<sub>anti</sub>**, the lower yield of **2<sub>syn</sub>** can be anticipated considering the higher relative energy of **2<sub>syn</sub>** by 7.3 kJ/mol (Supporting Information Figure S36).<sup>a</sup>

### Conformation-modulated reactivity

The major structural difference between the isomeric dimers **2<sub>anti</sub>** and **2<sub>syn</sub>** lies in their distinct *transoid* and *cisoid* conformations. These may serve as ideal artificial prototypes to understand the conformation-dependent chemical reactivities. Interestingly, dimer **2<sub>anti</sub>** readily undergoes a further oxidative fusion reaction to acquire **4<sub>anti</sub>** (Supporting Information Figure S28) in a high yield of 91% by linking C1 and C8' from pyrroles A and B', respectively (Scheme 2). In contrast, treatment of **2<sub>syn</sub>** with various oxidants only afforded undefined



**Scheme 2** | Structure of the proposed intermediate to afford multiply-fused compound **4<sub>anti</sub>**. Reaction conditions: (i) p-chloranil in toluene; (ii) DDQ in  $CH_2Cl_2$ , Ar =  $C_6F_5$ . The fluorine atoms attached to rings F/F' within **4<sub>anti</sub>** are omitted for clarity.

DOI: 10.31635/ccschem.023.202202690

Citation: CCS Chem. 2023, 5, 1332–1342

Link to VoR: <https://doi.org/10.31635/ccschem.023.202202690>

complicated mixtures. In the structure of **4<sub>anti</sub>**, the two monomeric units are further linked between the sp<sup>3</sup> C1 and sp<sup>2</sup> C8' to form a seven-membered ring H in a nonplanar envelope conformation (Figure 2d,h,l and Scheme 2). As a result, a unique [6.5.5.7.5.5.6]-octacyclic fused ring structure is formed, incorporating a roughly planar bipyrrolo-indolylidene core associated with the confused pyrrole A (Supporting Information Figure S33). The <sup>1</sup>H NMR spectrum of **4<sub>anti</sub>** exhibits an unsymmetrical structural feature; a lack of a confused pyrrole NH peak and a shift of the  $\alpha$ -CH of the same ring to the deshielded region ( $\delta = 8.36$  ppm) are observed (Supporting Information Figures S18-S21). In addition, the sp<sup>3</sup>-hybridized carbon (C1) signal resonates at 84.39 ppm in the <sup>13</sup>C NMR spectrum (Supporting Information Figure S22).

The different reactivity for **2<sub>anti</sub>** and **2<sub>syn</sub>** may be ascribed to their distinct conformations. In **2<sub>anti</sub>**, the reactive A and A' rings are tilted from the planar FGB-B'G'F' moiety with dihedral angles of 60.8° and 69.5°, affording short C1...C8' and C8...C1' distances of 3.222(6) and 3.332(6) Å, respectively (Figure 2i). In contrast, the larger A/B' and B/A' dihedral angles of 111.8° and 88.6° in **2<sub>syn</sub>** lead to longer C1...C8' and C8...C1' distances of 3.705(1) and 3.408(1) Å, respectively (Figure 2j). Thus, the different reactivity of **2<sub>anti</sub>** and **2<sub>syn</sub>** is attributable to the distances between the reactive sites, constrained by the alignments of the macrocycles around the central core. Notably, the exclusive formation of dimer **4<sub>anti</sub>** among the potential

isomers indicates that **4<sub>anti</sub>** is an energetically favored isomer compared to the potential ones with different linking modes (C2-C8' and N1-C8') (Supporting Information Figure S37). Notably, **4<sub>anti</sub>** also exhibits much lower relative energy (35.2 kJ/mol) than its hypothetical syn-isomer **4<sub>syn</sub>**, indicating that **4<sub>syn</sub>** is extremely unstable, consistent with the observation that **4<sub>syn</sub>** cannot be synthesized from **2<sub>syn</sub>**.

#### UV-vis-NIR absorption spectra and acid response

The absorption spectra of **1-4** were recorded in CH<sub>2</sub>Cl<sub>2</sub> (Figure 4a). Thia-hydrosapphyrin **1** displays an intense Soret-like peak centered at 418 nm and a broad NIR band in the 600–950 nm range. Upon dimerization, the isomeric dimers **2<sub>anti</sub>**, **2<sub>syn</sub>**, and fused **4<sub>anti</sub>** demonstrate considerably broadened absorption bands in the visible region. In contrast, the absorption spectrum of **3** exhibits a relatively sharp spectral feature with a less-intense red-to-NIR band ( $\lambda_{\text{max}} = 698$  nm), resulting from its partially disrupted  $\pi$ -conjugation at the sp<sup>3</sup> C5 and C5' atoms. Based on the respective onset wavelengths of 990, 1225, 1270, 900, and 1180 nm observed for **1**, **2<sub>anti</sub>**, **2<sub>syn</sub>**, **3**, and **4<sub>anti</sub>**, their optical band gaps were calculated to be 1.25, 1.01, 0.98, 1.38, and 1.05 eV, respectively (Supporting Information Figure S35), in a sequence which is not fully consistent with that of the density functional theory (DFT) calculated highest occupied molecular orbital

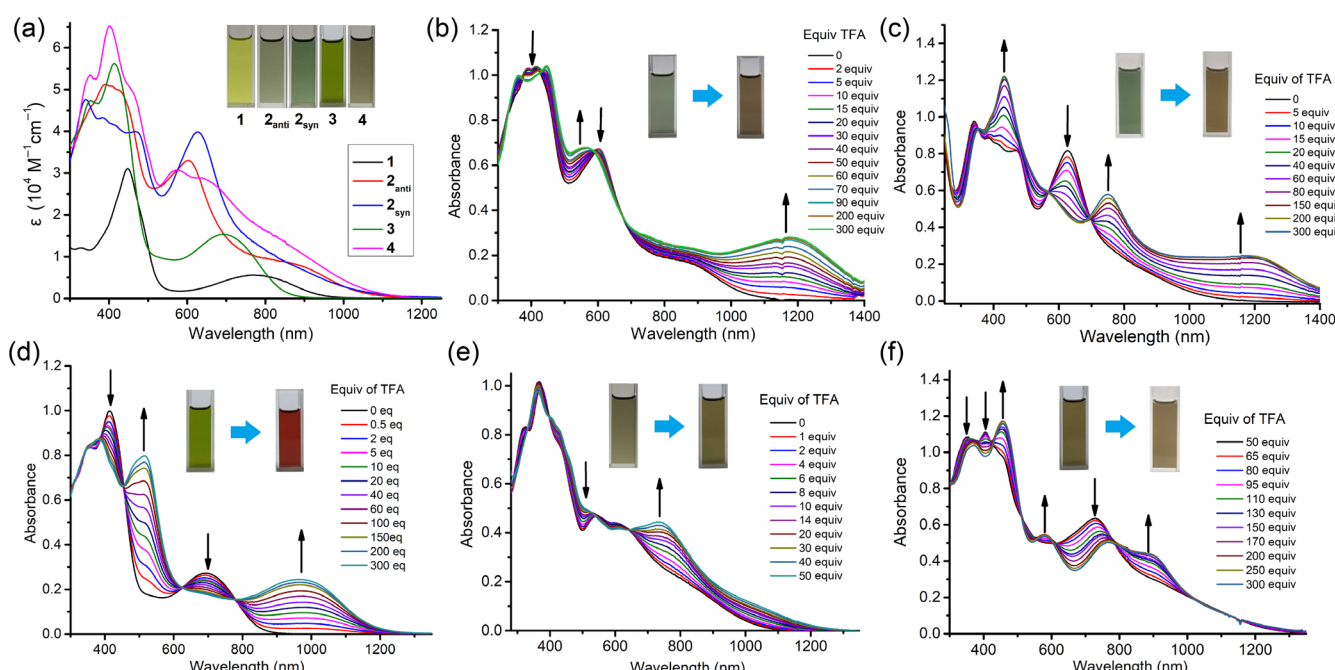


**Figure 4 |** UV-vis-NIR absorption spectra of **1**, **2<sub>anti</sub>**, **2<sub>syn</sub>**, **3**, and **4<sub>anti</sub>** in CH<sub>2</sub>Cl<sub>2</sub> (a). Insets: photographs of the solutions. The absorption spectral changes during the addition of TFA (0–300 equiv) to the solutions of **2<sub>anti</sub>** (b), **2<sub>syn</sub>** (c), **3** (d), and **4<sub>anti</sub>** (e, f) (20  $\mu$ M in CH<sub>2</sub>Cl<sub>2</sub>).

DOI: 10.31635/ccschem.023.202202690

Citation: CCS Chem. 2023, 5, 1332–1342

Link to VoR: <https://doi.org/10.31635/ccschem.023.202202690>

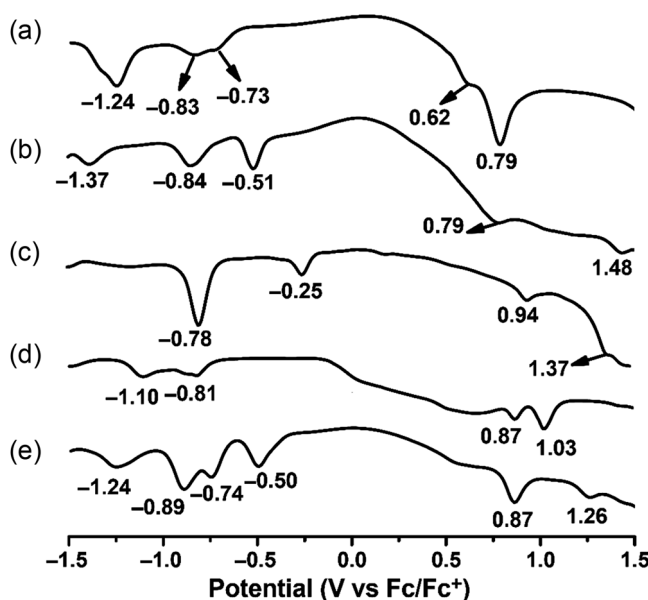


**Figure 5 |** Differential pulse voltammograms of **1** (a), **2<sub>anti</sub>** (b), **2<sub>syn</sub>** (c), **3** (d), and **4<sub>anti</sub>** (e) measured in anhydrous CH<sub>2</sub>Cl<sub>2</sub> containing 0.1 M tetra-*n*-butylammonium perchlorate as the supporting electrolyte.

(HOMO)-lowest unoccupied molecular orbital (LUMO) gaps in the vacuum approximation (Supporting Information Tables S2 and S3). However, time-dependent DFT calculations of the molecules accounting for solvent effects of CH<sub>2</sub>Cl<sub>2</sub> using the polarizable continuum model simulated well the optical spectra and optical band gaps. Thus, the lowest-energy-lying absorption bands mainly corresponding to HOMO-LUMO transitions were calculated to be 825, 1118, 1165, 715, and 1109 nm for **1**, **2<sub>anti</sub>**, **2<sub>syn</sub>**, **3**, and **4<sub>anti</sub>**, respectively, in the same sequence revealed by the optical band gaps (Supporting Information Figures S39–S43 and Tables S4–S8). In addition to the absorption spectra, the fluorescence spectra of these compounds were also measured. They are all nonfluorescent, which may be related to the occurrence of nonradiative transitions facilitated by their rather flexible and twisted conformations. Notably, upon the gradual addition of trifluoroacetic acid (TFA) to the solution of **2<sub>anti</sub>** (and **2<sub>syn</sub>**), the deep NIR absorption band beyond 1200 nm was intensified (Figure 4b,c). Similarly, an intensified NIR absorption band was also observed for **3** upon adding TFA, accompanied by a vivid color change from light green to wine red (Figure 4d). These changes could have resulted from the protonation at the imino-nitrogen sites in the arch subunits. In contrast, a two-step protonation process was likely observed for the unsymmetrical dimer **4<sub>anti</sub>**, which implied different basicity of the nitrogen sites in ring A and the arch's pyrroles (Figure 4e,f). The acid-induced spectral changes of these derivatives may be applicable in acid-responsive sensing in the NIR region.

## Electrochemistry

The electrochemical properties of the dimers were studied using cyclic voltammetry and differential pulse voltammetry in CH<sub>2</sub>Cl<sub>2</sub> containing 0.1 M tetra-*n*-butylammonium perchlorate (TBAClO<sub>4</sub>) as the supporting electrolyte (Figure 5a–e and Supporting Information Figure S44 and Table S9). The thia-hydrosapphirin **1** demonstrated two quasi-reversible oxidation waves at 0.62 and 0.79 V and three irreversible reduction peaks at −0.73, −0.83, and −1.24 V. Compared to **1**, the first reduction potentials of the *transoid* isomers of **2<sub>anti</sub>** and **2<sub>syn</sub>** were −0.51 and −0.25 V, respectively, which are remarkably anodically shifted compared to that of **1**. In contrast, the non-fully conjugated *cisoid* dimer **3** showed a cathodically shifted first reduction potential (−0.81 V). In addition, the multiply fused dimer **4<sub>anti</sub>** exhibited split reduction potentials at −0.50, −0.74, −0.89, and −1.24 V, respectively, which may result from its highly unsymmetrical structure. In contrast, the oxidation potentials of **2–4** were all anodically shifted compared to **1**, which were detected at 0.79, 0.94, 0.87, and 0.87 V, respectively. Compared to **2<sub>anti</sub>**, the relatively positive first oxidation potential of **2<sub>syn</sub>** may partly rationalize its resistance toward oxidation to afford the corresponding fused dimer **4<sub>syn</sub>** like **4<sub>anti</sub>** (Supporting Information Figure S37). Based on the data above, the corresponding electrochemical HOMO–LUMO energy gaps of **2<sub>anti</sub>**, **2<sub>syn</sub>**, **3**, and **4<sub>anti</sub>** were determined to be 1.30, 1.19, 1.68, and 1.37 V, respectively, in the same sequence as their optical band gaps (vide supra).

## Conclusion

Here, we have successfully constructed thia-sapphirin dimers bearing multiply fused heteroaromatic rings as effective artificial platforms to reveal the importance of conformation-governed chemical reactivity for constructing complex macrocycle arrays. Thus, the oxidative fusion of thia-hydrosapphirin **1** afforded stereo-dependent dimeric compounds, **2<sub>anti</sub>**, **2<sub>syn</sub>**, and **3** through the intrinsic radical-mediated coupling of aza-benzopentalenylidene moieties. Incorporating a terminal thiophene ring into the sapphirin scaffold considerably altered the oxidative reactivity. The resulting isomeric dimers **2<sub>anti</sub>** and **2<sub>syn</sub>** with two π-conjugated straps lying at the opposite (*anti*) and same (*syn*) sides of the cores exhibit dramatically different chemical reactivities. Dimer **2<sub>anti</sub>** can be readily oxidized to afford **4<sub>anti</sub>** comprising a coplanar annulated [6.5.5.7.5.5.6]-octacyclic framework in a high yield. In contrast, further oxidation of **2<sub>syn</sub>** only resulted in complicated undefined mixtures. All the fused products showed efficient light-harvesting ability and an acid-sensitive nature. These results demonstrate unique examples of synthesizing π-conjugated porphyrinoid dimers, highlighting the importance of conformation-modulated reactivity, which may compose an approach for constructing 3D-twisted

porphyrin analog arrays and the related functional molecules toward NIR-light applications.

## Footnote

<sup>a</sup> All calculations were performed with the Gaussian16 program package. See the Supporting Information for more details.

## Supporting Information

Supporting Information is available and includes experimental details, NMR and HRMS data, supplementary crystal and crystallographic data, supplementary electrochemical data, and DFT-computational data.

## Conflict of Interest

There is no conflict of interest to report.

## Funding Information

This research at ECUST was financially supported by the Shanghai Municipal Science and Technology Major Project (grant no. 2018SHZDZX03), the International Cooperation Program of Shanghai Science and Technology Committee (grant no. 17520750100), NSFC (grant nos. 22131005, 22201074, 21971063, and 22075077), Program of Introducing Talents of Discipline to Universities (grant no. B16017), the Fundamental Research Funds for the Central Universities (grant no. 222201717003), Program of Shanghai Academic Research Leader (grant no. 20XD1401400), and Natural Science Foundation of Shanghai (grant nos. 22ZR1416100 and 20ZR1414100). The work in TMU was supported by a JST PRESTO (grant no. JPMJPR2103), and in Kyushu was endorsed by a Grants-in-Aid (grant nos. JP20H00406 and JP21K18984) from the Japan Society for the Promotion of Science (JSPS). G.B. thanks the Swedish National Infrastructure for Computing (SNIC) resources at the High-Performance Computing Center North (HPC2N) and the financial support of the Swedish Research Council (grant nos. 2018-05973 and 2020-04600).

## Acknowledgments

The authors thank the Research Center of Analysis and Test of East China University of Science and Technology for compound characterization.

## References

- D'Angelo, K. A.; Schissel, C. K.; Pentelute, B. L.; Movassaghi, M. Total Synthesis of Himastatin. *Science* **2022**, *375*, 894-899.
- Sugiyama, R.; Suarez, A. F. L.; Morishita, Y.; Nguyen, T. Q. N.; Tooh, Y. W.; Roslan, M. N. H. B.; Lo Choy, J.; Su, Q.; Goh, W. Y.; Gunawan, G. A.; Wong, F. T.; Morinaka, B. I. The Biosynthetic Landscape of Triceptides Reveals Radical SAM Enzymes That Catalyze Cyclophane Formation on Tyr- and His-Containing Motifs. *J. Am. Chem. Soc.* **2022**, *144*, 11580-11593.
- Dengler, S.; Douat, C.; Huc, I. Differential Peptide Multi-Macrocyclizations at the Surface of a Helical Foldamer Template. *Angew. Chem. Int. Ed.* **2022**, *61*, e202211138.
- Zhang, W.; Li, L.; Li, C.-C. Synthesis of Natural Products Containing Highly Strained *Trans*-Fused Bicyclo[3.3.0]Octane: Historical Overview and Future Prospects. *Chem. Soc. Rev.* **2021**, *50*, 9430-9442.
- Sun, J.; Yang, H.; Tang, W. Recent Advances in Total Syntheses of Complex Dimeric Natural Products. *Chem. Soc. Rev.* **2021**, *50*, 2320-2336.
- Satoh, H.; Manabe, S. Design of Chemical Glycosyl Donors: Does Changing Ring Conformation Influence Selectivity/Reactivity? *Chem. Soc. Rev.* **2013**, *42*, 4297-4309.
- Schnitzer, T.; Wennemers, H. Influence of the *Trans/Cis* Conformer Ratio on the Stereoselectivity of Peptidic Catalysts. *J. Am. Chem. Soc.* **2017**, *139*, 15356-15362.
- Dosso, J.; Bartolomei, B.; Demitri, N.; Cossío, F. P.; Prato, M. Phenanthrene-Extended Phenazine Dication: An Electrochromic Conformational Switch Presenting Dual Reactivity. *J. Am. Chem. Soc.* **2022**, *144*, 7295-7301.
- Crich, D.; Banerjee, A. Chemistry of the Hexahydropyrrolo[2,3-*b*]indoles: Configuration, Conformation, Reactivity, and Applications in Synthesis. *Acc. Chem. Res.* **2007**, *40*, 151-161.
- Kadish, K. M., Smith, K. M., Guilard, R., Eds.; *The Porphyrin Handbook*; Academic Press: San Diego, CA, **2000**, Vol. 1-20.
- Kadish, K. M., Smith, K. M., Guilard, R., Eds.; *Heme Biochemistry in Handbook of Porphyrin Science*; World Scientific: Singapore, **2013**, Vol. 26.
- Kadish, K. M., Smith, K. M., Guilard, R., Eds.; *Guillard Chlorophyll, Photosynthesis and Bio-Inspired Energy in Handbook of Porphyrin Science*; World Scientific: Singapore, **2013**, Vol. 28.
- Jing, H.; Rong, J.; Taniguchi, M.; Lindsey, J. S. Phenylene-Linked Tetrapyrrole Arrays Containing Free Base and Diverse Metal Chelate Forms – Versatile Synthetic Architectures for Catalysis and Artificial Photosynthesis. *Coord. Chem. Rev.* **2022**, *456*, 214278.
- Tanaka, T.; Osuka, A. Conjugated Porphyrin Arrays: Synthesis, Properties and Applications For Functional Materials. *Chem. Soc. Rev.* **2015**, *44*, 943-969.
- Luo, J.; Lee, S.; Son, M.; Zheng, B.; Huang, K.-W.; Qi, Q.; Zeng, W.; Li, G.; Kim, D.; Wu, J. N-Annulated Perylene-Substituted and Fused Porphyrin Dimers with Intense Near-Infrared One-Photon and Two-Photon Absorption. *Chem. Eur. J.* **2015**, *21*, 3708-3715.
- Mori, H.; Tanaka, T.; Lee, S.; Lim, J. M.; Kim, D.; Osuka, A. Meso-meso Linked Porphyrin-[26]Hexaphyrin-Porphyrin Hybrid Arrays and Their Triply Linked Tapes Exhibiting

- Strong Absorption Bands in the NIR Region. *J. Am. Chem. Soc.* **2015**, *137*, 2097–2106.
17. Yoshida, N.; Shimidzu, H.; Osuka, A. Meso-Meso Linked Diporphyrins from 5,10,15-Trisubstituted Porphyrins. *Chem. Lett.* **1998**, *27*, 55–56.
18. Ogawa, T.; Nishimoto, Y.; Yoshida, N.; Ono, N.; Osuka, A. Completely Regioselective Synthesis of Directly Linked meso,meso and meso, $\beta$  Porphyrin Dimers by One-Pot Electrochemical Oxidation of Metalloporphyrins. *Angew. Chem. Int. Ed.* **1999**, *38*, 176–179.
19. Hata, H.; Shinokubo, H.; Osuka, A. Highly Regioselective Ir-Catalyzed  $\beta$ -Borylation of Porphyrins via C–H Bond Activation and Construction of  $\beta$ – $\beta$ -Linked Diporphyrin. *J. Am. Chem. Soc.* **2005**, *127*, 8264–8265.
20. Aratani, N.; Osuka, A. Exploration of Giant Functional Porphyrin Arrays. *Bull. Chem. Soc. Jpn.* **2014**, *88*, 1–27.
21. Van Raden, J. M.; Alexandropoulos, D. I.; Slota, M.; Sopp, S.; Matsuno, T.; Thompson, A. L.; Isobe, H.; Anderson, H. L.; Bogani, L. Singly and Triply Linked Magnetic Porphyrin Lanthanide Arrays. *J. Am. Chem. Soc.* **2022**, *144*, 8693–8706.
22. Grzybowski, M.; Sadowski, B.; Butenschön, H.; Gryko, D. T. Synthetic Applications of Oxidative Aromatic Coupling—From Biphenols to Nanographenes. *Angew. Chem. Int. Ed.* **2020**, *59*, 2998–3027.
23. Stępień, M.; Gońska, E.; Żyła, M.; Sprutta, N. Heterocyclic Nanographenes and Other Polycyclic Heteroaromatic Compounds: Synthetic Routes, Properties, and Applications. *Chem. Rev.* **2017**, *117*, 3479–3716.
24. Kato, K.; Osuka, A. Platforms for Stable Carbon-Centered Radicals. *Angew. Chem. Int. Ed.* **2019**, *58*, 8978–8986.
25. Shimizu, D.; Osuka, A. Porphyrinoids as a Platform of Stable Radicals. *Chem. Sci.* **2018**, *9*, 1408–1423.
26. Togano, M.; Furuta, H. Blooming of Confused Porphyrinoids—Fusion, Expansion, Contraction, and More Confusion. *Chem. Commun.* **2012**, *48*, 937–954.
27. Szyszko, B.; Bialek, M. J.; Pacholska-Dudziak, E.; Latos-Grajski, L. Flexible Porphyrinoids. *Chem. Rev.* **2017**, *117*, 2839–2909.
28. Li, Q.; Ishida, M.; Wang, Y.; Li, C.; Baryshnikov, G.; Zhu, B.; Sha, F.; Wu, X.; Ågren, H.; Furuta, H.; Xie, Y. Antiaromatic Sapphyrin Isomer: Transformation into Contracted Porphyrinoids with Variable Aromaticity. *Angew. Chem. Int. Ed.* **2023**, *62*, e202212174.
29. Togano, M.; Furuta, H. Creation from Confusion and Fusion in the Porphyrin World—The Last Three Decades of N-Confused Porphyrinoid Chemistry. *Chem. Rev.* **2022**, *122*, 8313–8437.
30. Su, G.; Li, Q.; Ishida, M.; Li, C.; Sha, F.; Wu, X.-Y.; Wang, L.; Baryshnikov, G.; Li, D.; Ågren, H.; Furuta, H.; Xie, Y. N-Confused Phlorin-Prodigiosin Chimera: meso-Aryl Oxidation and  $\beta$ -Extension Triggered by Peripheral Coordination. *Angew. Chem. Int. Ed.* **2020**, *59*, 1537–1541.
31. Li, C.; Li, Q.; Shao, J.; Tong, Z.; Ishida, M.; Baryshnikov, G.; Ågren, H.; Furuta, H.; Xie, Y. Expanded N-Confused Phlorin: A Platform for a Multiply Fused Polycyclic Ring System via Oxidation Within the Macrocycle. *J. Am. Chem. Soc.* **2020**, *142*, 17195–17205.
32. Xie, Y.; Wei, P.; Li, X.; Hong, T.; Zhang, K.; Furuta, H. Macrocycle Contraction and Expansion of a Dihydrosapphyrin Isomer. *J. Am. Chem. Soc.* **2013**, *135*, 19119–19122.
33. Furuta, H.; Asano, T.; Ogawa, T. “N-Confused Porphyrin”: A New Isomer of Tetraphenylporphyrin. *J. Am. Chem. Soc.* **1994**, *116*, 767–768.
34. Chmielewski, P. J.; Latos-Grajski, L.; Rachlewicz, K.; Głowiąk, T. Tetra-*p*-Tolylporphyrin with an Inverted Pyrrole Ring: A Novel Isomer of Porphyrin. *Angew. Chem. Int. Ed. Engl.* **1994**, *33*, 779–781.
35. Furuta, H.; Ishizuka, T.; Osuka, A.; Ogawa, T. “N-Fused Porphyrin” from N-Confused Porphyrin. *J. Am. Chem. Soc.* **1999**, *121*, 2945–2946.
36. Furuta, H.; Ishizuka, T.; Osuka, A.; Ogawa, T. “N-Fused Porphyrin”: A New Tetrapyrrolic Porphyrinoid with a Fused Tri-pentacyclic Ring. *J. Am. Chem. Soc.* **2000**, *122*, 5748–5757.
37. Togano, M.; Kimura, T.; Uno, H.; Furuta, H. Doubly N-Fused Porphyrin. *Angew. Chem. Int. Ed.* **2008**, *47*, 8913–8916.
38. Togano, M.; Furuta, H. N-Fused Porphyrin: A Maverick Member of the Porphyrin Family. *Chem. Lett.* **2019**, *48*, 615–622.
39. Pushpanandan, P.; Grover, V.; Ravikanth, M. Synthesis of meso-Triaryl 22-Oxanorroles. *Org. Lett.* **2022**, *24*, 3184–3188.
40. Li, M.; Wei, P.; Ishida, M.; Li, X.; Savage, M.; Guo, R.; Ou, Z.; Yang, S.; Furuta, H.; Xie, Y. Macroyclic Transformations from Norrole to Isonorrole and an N-Confused Corrole with a Fused Hexacyclic Ring System Triggered by a Pyrrole Substituent. *Angew. Chem. Int. Ed.* **2016**, *55*, 3063–3067.
41. Fujino, K.; Hirata, Y.; Kawabe, Y.; Morimoto, T.; Srinivasan, A.; Togano, M.; Miseki, Y.; Kudo, A.; Furuta, H. Confusion and Neo-Confusion: Corrole Isomers with an NNNC Core. *Angew. Chem. Int. Ed.* **2011**, *50*, 6855–6859.
42. Togano, M.; Kawabe, Y.; Furuta, H. C-Fused Norrole: A Fused Corrole Isomer Bearing a N,C-Linked Bipyrrole Unit. *J. Org. Chem.* **2011**, *76*, 7618–7622.
43. Wei, P.; Zhang, K.; Li, X.; Meng, D.; Ågren, H.; Ou, Z.; Ng, S.; Furuta, H.; Xie, Y. Neo-Fused Hexaphyrin: A Molecular Puzzle Containing an N-Linked Pentaphyrin. *Angew. Chem. Int. Ed.* **2014**, *53*, 14069–14073.
44. Gao, S.; Li, Q.; Baryshnikov, G.; Ågren, H.; Xie, Y. Synthesis, Characterization, and Spectroscopic Properties of 2-(3,5,6-Trichloro-1,4-benzoquinon-2-yl)-neo-fused Hexaphyrin. *Bull. Korean Chem. Soc.* **2021**, *42*, 1569–1573.
45. Ishizuka, T.; Osuka, A.; Furuta, H. Inverted N-Confused Porphyrin Dimer. *Angew. Chem. Int. Ed.* **2004**, *43*, 5077–5081.
46. Togano, M.; Kawabe, Y.; Uno, H.; Furuta, H. Unique Interaction Between Directly Linked Laminated  $\pi$  Planes in the Benzonorrole Dimer. *Angew. Chem. Int. Ed.* **2012**, *51*, 8753–8756.
47. Li, Q.; Li, C.; Baryshnikov, G.; Ding, Y.; Zhao, C.; Gu, T.; Sha, F.; Liang, X.; Zhu, W.; Wu, X.; Ågren, H.; Sessler, J. L.; Xie, Y. Twisted-Planar-Twisted Expanded Porphyrinoid Dimer as a Rudimentary Reaction-Based Methanol Indicator. *Nat. Commun.* **2020**, *11*, 5289.

48. Chmielewski, P. J. Synthesis and Characterization of a Directly Linked N-Confused Porphyrin Dimer. *Angew. Chem. Int. Ed.* **2004**, *43*, 5655–5658.
49. Moreira, L.; Calbo, J.; Aragó, J.; Illescas, B. M.; Nierengarten, I.; Delavaux-Nicot, B.; Ortí, E.; Martín, N.; Nierengarten, J.-F. Conjugated Porphyrin Dimers: Cooperative Effects and Electronic Communication in Supramolecular Ensembles with C<sub>60</sub>. *J. Am. Chem. Soc.* **2016**, *138*, 15359–15367.
50. Li, Q.; Li, C.; Kim, J.; Ishida, M.; Li, X.; Gu, T.; Liang, X.; Zhu, W.; Ågren, H.; Kim, D.; Furuta, H.; Xie, Y. Regioselectively Halogenated Expanded Porphyrinoids as Building Blocks for Constructing Porphyrin-Porphyrinoid Heterodyads with Tunable Energy Transfer. *J. Am. Chem. Soc.* **2019**, *141*, 5294–5302.
51. Gupta, I.; Srinivasan, A.; Morimoto, T.; Togano, M.; Furuta, H. N-Confused and N-Fused *meso*-Aryl Sapphyrins. *Angew. Chem. Int. Ed.* **2008**, *47*, 4563–4567.
52. Inokuma, Y.; Matsunari, T.; Ono, N.; Uno, H.; Osuka, A. A Doubly N-Fused Benzohexaphyrin and Its Rearrangement to a Fluorescent Macrocycle Upon DDQ Oxidation. *Angew. Chem. Int. Ed.* **2005**, *44*, 1856–1860.
53. Higashino, T.; Inoue, M.; Osuka, A. Singly N-Fused Möbius Aromatic [28]Hexaphyrins(1.1.1.1.1). *J. Org. Chem.* **2010**, *75*, 7958–7961.
54. Hafner, K.; Schmidt, F. A Stable 2-Azapentalene. *Angew. Chem. Int. Ed. Engl.* **1973**, *12*, 418–419.
55. Gadekar, S. C.; Reddy, B. K.; Anand, V. G. Metal-Assisted Cyclomerization of N-Confused Dipyrromethanes into Expanded Norroles. *Angew. Chem. Int. Ed.* **2013**, *52*, 7164–7167.
56. Bröring, M.; Köhler, S.; Kleeberg, C. Norcorrole: Observation of the Smallest Porphyrin Variant with a N<sub>4</sub> Core. *Angew. Chem. Int. Ed.* **2008**, *47*, 5658–5660.
57. Schweyen, P.; Hoffmann, M.; Krumsiek, J.; Wolfram, B.; Xie, X.; Bröring, M. Metal-Assisted One-Pot Synthesis of Isoporphyrin Complexes. *Angew. Chem. Int. Ed.* **2016**, *55*, 10118–10121.
58. Omori, H.; Hiroto, S.; Takeda, Y.; Fliegl, H.; Minakata, S.; Shinokubo, H. Ni(II) 10-Phosphacorrole: A Porphyrin Analogue Containing Phosphorus at the Meso Position. *J. Am. Chem. Soc.* **2019**, *141*, 4800–4805.
59. Chen, Z.; Wannere, C. S.; Corminboeuf, C.; Puchta, R.; Schleyer, P. v. R. Nucleus-Independent Chemical Shifts (NICS) as an Aromaticity Criterion. *Chem. Rev.* **2005**, *105*, 3842–3888.
60. Geuenich, D.; Hess, K.; Köhler, F.; Herges, R. Anisotropy of the Induced Current Density (ACID), a General Method to Quantify and Visualize Electronic Delocalization. *Chem. Rev.* **2005**, *105*, 3758–3772.